

Effect of Substrate and Nanoparticle Spacing on Plasmonic Enhancement in Three-Dimensional Nanoparticle Structures

Anil Yuksel

Department of Mechanical Engineering,
The University of Texas at Austin,
Austin, TX 78712
e-mail: anil.yuksel@utexas.edu

Edward T. Yu

Microelectronics Research Center,
Department of Electrical and
Computer Engineering,
The University of Texas at Austin,
Austin, TX 78712

Jayathi Murthy

Henry Samueli School of Engineering and
Applied Science,
University of California, Los Angeles,
Los Angeles, CA 90095

Michael Cullinan

Department of Mechanical Engineering,
The University of Texas at Austin,
Austin, TX 78712

Surface plasmon polaritons associated with light-nanoparticle interactions can result in dramatic enhancement of electromagnetic fields near and in the gaps between the particles, which can have a large effect on the sintering of these nanoparticles. For example, the plasmonic field enhancement within nanoparticle assemblies is affected by the particle size, spacing, interlayer distance, and light source properties. Computational analysis of plasmonic effects in three-dimensional (3D) nanoparticle packings are presented herein using 532 nm plane wave light. This analysis provides insight into the particle interactions both within and between adjacent layers for multilayer nanoparticle packings. Electric field enhancements up to 400-fold for transverse magnetic (TM) or X-polarized light and 26-fold for transverse electric (TE) or Y-polarized light are observed. It is observed that the thermo-optical properties of the nanoparticle packings change nonlinearly between 0 and 10 nm gap spacing due to the strong and nonlocal near-field interaction between the particles for TM polarized light, but this relationship is linear for TE polarized light. These studies help provide a foundation for understanding micro/nanoscale heating and heat transport for Cu nanoparticle packings under 532 nm light under different polarization for the photonic sintering of nanoparticle assemblies.

[DOI: 10.1115/1.4037770]

Keywords: nanotechnology, near-field thermal energy enhancement, laser heating

Introduction

With the recent growth of the field of printed electronics, photonic sintering on metal nanoparticles has started to gain significant attention [1,2]. In these systems, nanoparticles are generally deposited on to a substrate and self-organize into three-dimensional (3D) packing structures. A high-intensity laser is then used to heat the nanoparticles and cause them to fuse together in order to create conductive, electronic structures [3,4]. However, the light-matter interactions for three-dimensional nanoparticle packings are not well understood. This is because upon illumination of the nanoparticles with a laser light source at certain wavelengths, polarizations, and incident angles, the optical reflectivity and absorption of the nanoparticle packing is strongly influenced by the type and size of the nanoparticle as well as the interparticle spacing [5]. Metal nanoparticles show unique plasmonic behavior under illumination at particular wavelengths, which makes them particularly sensitive to the illumination and packing structure [6]. When metallic nanoparticles are dispersed in solvents, they exhibit very strong and localized surface plasmon resonance peaks, which are caused by the collective free electron oscillations in metal [7,8]. However, these dispersed particles do not have significant interactions with each other due to their large separation distances between particles in the dispersion. In a typical nanoparticle assembly used to make electronic interconnect structures, the nanoparticles are generally packed very close together that causes them to have significant particle-to-particle interactions. Therefore, this paper presents a study of how spacing between

particles affects the thermo-optical properties of the 3D packing structures.

Very few studies of nanoscale particle structures exist, but numerous continuum models of the macroscale photonic sintering process that approximate the nanoparticle assembly as a continuous medium have been developed [9–16]. In these models, the heat equation, along with a laser source term, is discretized across the domain using a finite element or finite volume mesh, and the resulting set of algebraic equations is solved to yield a prediction of the temperature distribution in the domain. This type of modeling approach works well when the optical, thermal, and melt/sintering properties of the assembly are well known. When parameters for particle assemblies cannot easily be measured experimentally, the discrete element method is commonly used. Discrete element method is a versatile technique for modeling particle assemblies in which each particle in a domain is represented as a sphere with certain geometric (position, radius) and thermal (temperature, conductivity, specific heat, emissivity) properties. Numerous models have been developed to predict the optical [17–21] and thermal [22–25] properties of nanoparticle assemblies. However, the physics of the photonic sintering process change as the particles in the assemblies become smaller than the wavelength of the laser used to sinter them.

Of the nanoscale particle assembly models that exist, they are generally configured into different periodic arrays of nanoparticles in two dimensions to demonstrate the electromagnetic coupling between the metallic nanoparticles. Well-ordered two-dimensional configuration analysis has been performed for many different applications; however, different 3D configurations are not well understood [26,27]. One of the main challenges in the analysis of 3D nanoparticle configurations is that the particles agglomerate with each other into poorly organized 3D configurations due to the van der Waals attraction between the particles. These van

Contributed by the Manufacturing Engineering Division of ASME for publication in the JOURNAL OF MICRO- AND NANO-MANUFACTURING. Manuscript received June 16, 2017; final manuscript received August 18, 2017; published online September 27, 2017. Assoc. Editor: Yayue Pan.

der Waals forces are a function of the size of the particles and interparticle spacing, as well as the surfactant properties in the nanoparticle solution [28,29]. Hence, understanding optical phenomena exhibited by metal nanoparticle packings such as surface plasmon resonance, light scattering, surface-enhanced Raman scattering [30], and light reflection in the optically thick and thin regimes is very crucial. Some optical and transmission electron microscopy images of thin metallic nanoparticle films on a substrate and corresponding X-ray diffraction patterns have shown that certain particle configurations are likely to arise depending on the deposition method [31]. Therefore, in this paper, we model a common 3D configuration with one nanoparticle sitting on top of three other nanoparticles. In addition, the recent studies on the size effect of surface plasmon resonance absorption have shown a shift in the resonance peak when the nanoparticle size increases in the size range of tens to hundreds of nanometers. Thus, in this paper, we analyze the extinction cross section of different Cu nanoparticle packings under laser illumination, focusing in particular on the time-averaged electromagnetic energy flux density with different 3D configurations for transverse electric (TE) and transverse magnetic (TM) polarization and its possible implications for nanoscale heating and thermal transport.

Modeling Analysis

In this paper, finite difference frequency domain simulations are applied to solve Maxwell's equations and analyze the effect of metallic nanoparticles spacing and packing on the near-field electromagnetic field intensity. Scattering from nanoparticles in the packing causes a perturbation to the total field induced by an incident plane wave. The total wave can be expressed as the superposition of the incident and scattered waves. Therefore, superposition of the incident wave, a reflected wave in the domain, and a transmitted wave in the substrate is necessary in order to analyze the metallic nanoparticle packings. Due to the fact that the scatterers are placed on a substrate, Maxwell's full field equation is solved without the presence of the scatterers that provide the entering background field to the domain for the scattered field analysis. To achieve this, one port in the simulation is set up ($E_0 = 1 \text{ V/m}$) to define the incident plane wave and the other port absorbs the transmitted wave. A perfectly matched layer outside of the computational region is used to absorb the scattered thermal radiation in all directions. The complex permittivity function of the metallic nanoparticles is taken from Johnson

and Christy [32] and the nanoparticles are placed onto a glass substrate ($n = 1.5$) and are surrounded with air ($n = 1$).

In this paper, both single nanoparticle (case *a*) and four nanoparticle configurations (case *b*) on a glass substrate are analyzed, as illustrated in Fig. 1. Since the nanoparticles exhibit different plasmonic effects at different gap distances, out-of-plane configurations need to be understood well in order to be able to tune the plasmonic optical properties of the nanoparticle assembly. Also, since nanoparticles tend to agglomerate at the nanoscale, the particles initially are modeled with an agglomerated configuration (case *b*) where all particles are all touching each other. These configurations are analyzed using both TM (*x*-polarized) and TE (*y*-polarized) plane wave illumination at a wavelength of 532 nm.

The nanoparticles used in this study are 100 nm diameter copper nanoparticles placed on a 350 nm thick, 750 nm \times 750 nm wide glass substrate. To be able to see the agglomeration effect in case *b*, the distance between the particles (*d*) is varied from 0 to 50 nm. By investigating TE and TM polarized light, scattering and absorption cross sections are calculated. The scattering cross section is found by calculating the surface integral of the scattered Poynting vector and the absorption cross section is analyzed by the volume integration of the absorbed energy within the nanoparticles.

Results and Discussion

Single Nanoparticle Analysis and Effect of Substrate. The cross-sectional analysis of a single particle on a glass substrate (case *a*) is shown in Fig. 1. Since the glass substrate is mostly transparent at 532 nm, and the 100 nm diameter copper nanoparticle does not create a strong near-field coupling within the gap between the particle and the glass substrate at 532 nm wavelength, it is observed that the maximum electric field enhancement $|E|/|E_0|$ is around 24 and increases slightly ($\sim 10\%$) as the gap increases from $d = 0$ to $d = 10$ nm. It can also be seen from Fig. 2 that the scattering cross section increases very slowly due to the small reflection from the glass substrate as the gap varies from 0 to 10 nm. The absorption cross section also increases with increasing gap distance; however, the maximum electromagnetic power loss density for the nanoparticle, which is located at the closest region of the nanoparticle to the glass substrate, decreases with as the gap size increases. This is expected since the nanoparticle and glass substrate are in thermal contact when $d = 0$, but the thermal coupling between the particle and the substrate decreases with

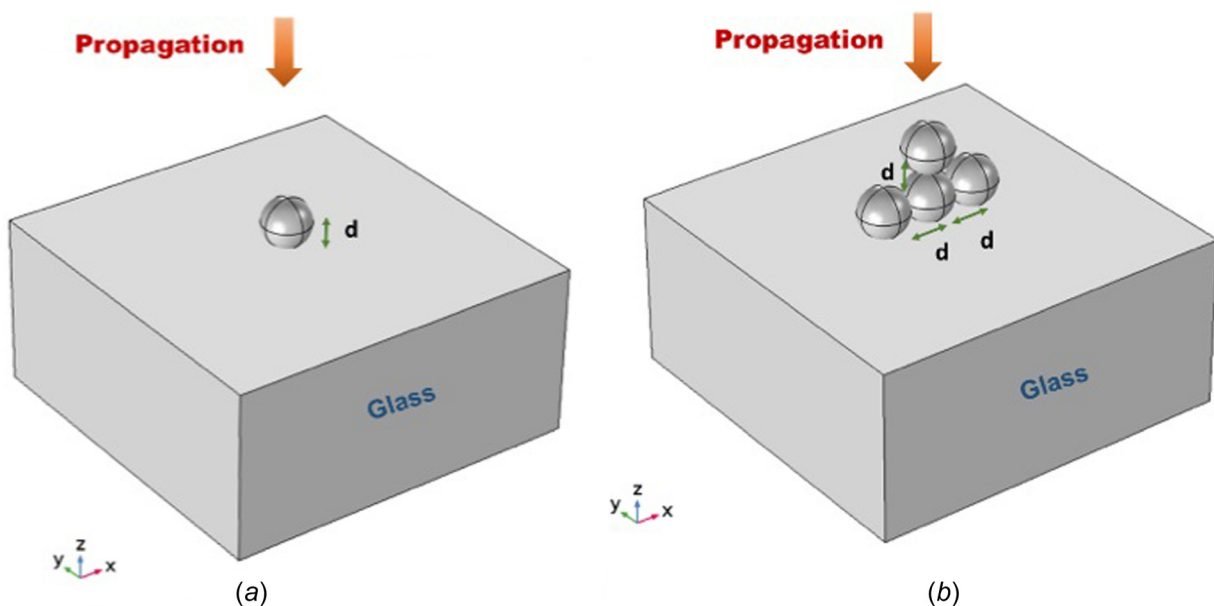


Fig. 1 Out of plane configurations: (a) single particle and (b) four particle

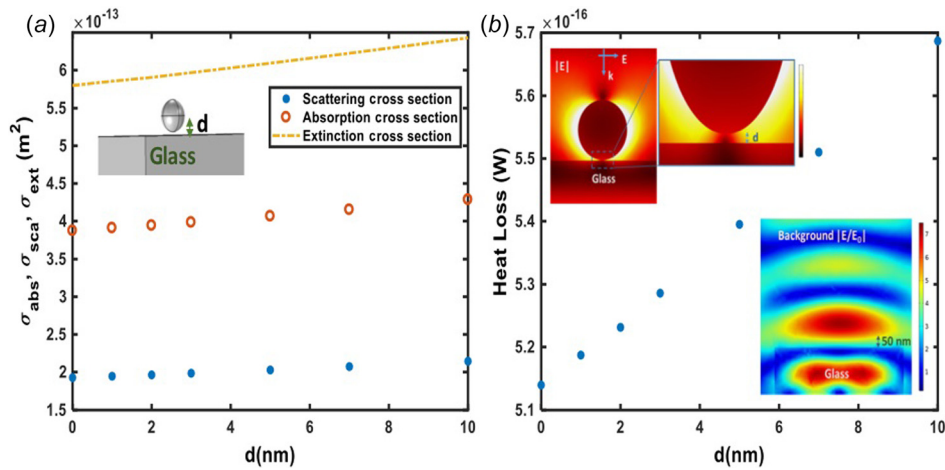


Fig. 2 Glass-copper nanoparticle: (a) absorption, scattering, and extinction cross section analysis of a single copper nanoparticle on a glass substrate and (b) the resistive heating loss in the copper nanoparticle on a glass substrate under $\lambda = 532$ nm, TM polarized (X-pol.) light with varying gap distance d and the background electric field norm

increased gap size. Nevertheless, volume integration of the absorbed energy results in increased absorption cross section with increasing gap. Hence, the extinction cross section also increases with increasing gap. Overall, it is observed that the absorption cross section is dominant over the scattering cross section for this particle size when placed on a glass substrate. In addition, the maximum electric field enhancement and heating loss both increase along the polarization direction for the nanoparticle above a glass substrate as the gap size increased from $d=0$ to $d=10$ nm. Furthermore, due to the small reflection by the glass substrate, the background field distribution around the nanoparticle and the relatively weak near-field coupling at the gap at 532 nm wavelength likely also affect this observed phenomena [33].

In order to analyze the effect of the substrate on the thermo-optical properties of the Cu nanoparticle, the scattering, absorption, and extinction cross section of a 100 nm diameter copper nanoparticle were also calculated without the glass substrate. From these simulations, it is observed that the maximum electric field enhancement near the edges of the copper nanoparticle caused by dipole mode is up to a factor of four. This means that the observed scattering, absorption, and extinction cross section values for the copper nanoparticle in air without a glass substrate

are around 35 times less than the values when the nanoparticle is placed on a glass substrate with $d=0$. Moreover, the heat loss observed for the simulations with an isolated single nanoparticle is also around 35 times less than the case where the single nanoparticle is placed on a glass substrate with $d=0$. This indicates that the even though the substrate is transparent to the light, it still has a significant effect on thermo-optical properties of the nanoparticles placed on the substrate and cannot be neglected in the analysis of the metal nanoparticle sintering in photonic sintering applications for electronics manufacturing.

Multiparticle Analysis and Effect of Interparticle Spacing for Transverse Magnetic Polarized Light. The TM polarized electric field enhancement for the nanoparticle configuration corresponding to case *b* when the particles are all in contact ($d=0$) is depicted in Fig. 3. It is observed that the electric field is enhanced up to 400 times between the adjacent nanoparticles, which is around 16 times higher than the case *a* when only one particle was sitting on the substrate. That shows that for copper nanoparticle packings with collinear nanoparticle packings, the incident field can drive the charge distribution in the metallic nanoparticles rapidly and create a plasmon waveguide for optical pulse propagation

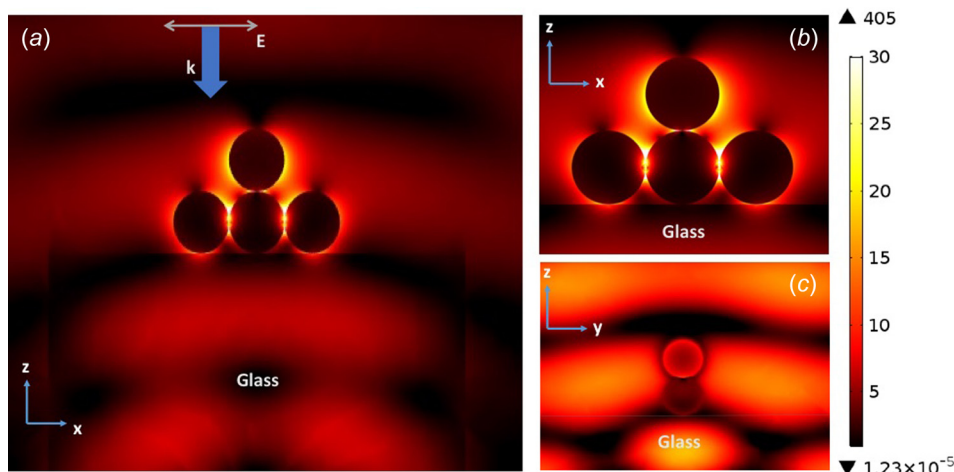


Fig. 3 Electric field enhancement $|E/E_0|$ for $d=0$ and $\lambda = 532$ nm, TM (X-pol.) polarized light (case *b*): (a) front view of electric field enhancement, (b) zoom view of nanoparticles in (a), and (c) side view of electric field enhancement

below diffraction limit [34,35]. It is also observed that the maximum enhancement occurs between the center nanoparticle in linear configuration and the adjacent particles. This is expected because there is a near-field coupling between the particles along the polarization direction combined with the localized plasmon resonance effect at 532 nm. This shows that a very strong localized field is generated below the diffraction limit. We also see that the particle above the three bottom particles has relatively weaker electric field enhancement than the adjacent particles in linear configuration due to the strong coupling along the polarization direction.

Figure 4 illustrates the effect on the electric field enhancement of varying the distance between the particles (d) between 10 nm and 50 nm for TM polarized light. It can be seen that the plasmonic effects are much more dominant along the direction of polarization and that the interaction between the nanoparticles of localized surface plasmon modes creates the gap modes. The effect of this very intense electromagnetic field is present when d is between 0 and 10 nm and the localized field is almost coherent between the adjacent particles with the contribution of the evanescent waves. Hence, it is expected that this strong electric field enhancement results in greater heating of the nanoparticles which will lead to more grain growth and neck formation between the particles. The electric field enhancement starts to decrease from a

factor of 64 to a factor of around 28 when d is decreased from 10 nm to 50 nm. This is expected due to the reduced near-field coupling between the particles. It is observed that the particle which is above the three bottom particles in a linear configuration does not affect the particles below. This is mostly due to the polarization effect, which results in generation of surface plasmon polaritons along the polarization direction. These results also show that the calculated field enhancement drops significantly as the gap spacing becomes very large. This makes sense because as the gap size increases beyond the radius of the particle, the particles start to behave individually and lose their strong plasmonic coupling effect. Hence, controlled coupling of localized and propagating modes is very promising way to tune electromagnetic energy transport for high sensitivity thermal systems.

Multiparticle Analysis and Effect of Interparticle Spacing for Transverse Electric Polarized Light.

The electric field enhancement with TE polarized light for the case b configuration when $d = 0$ is shown in Fig. 5. In this configuration, the electric field is enhanced more than 26 times between the adjacent nanoparticles, which is around 15 times less than when the same configuration is illuminated using TM polarized light. It is also observed that the maximum enhancement occurs along the

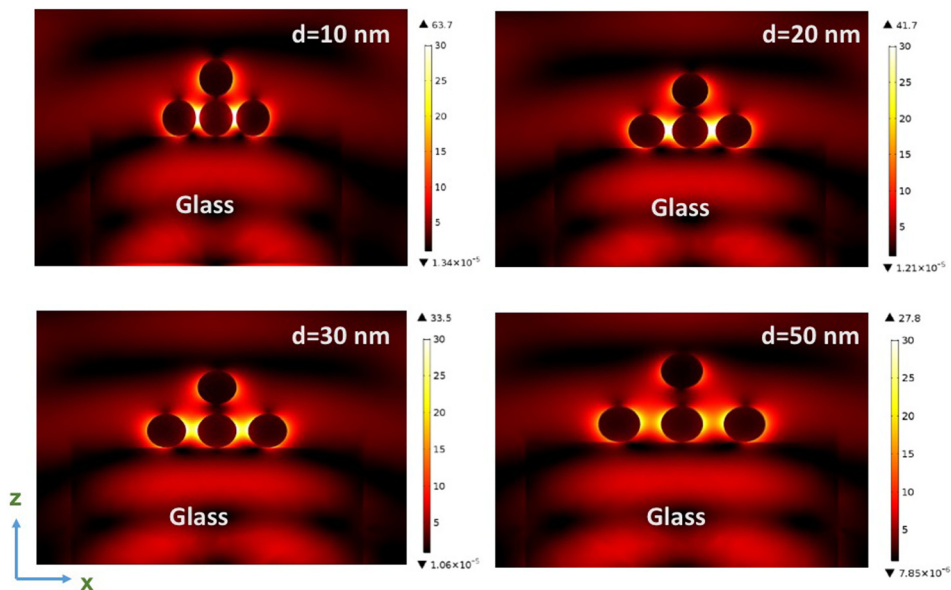


Fig. 4 Electric field enhancement $|E/E_0|$ with $\lambda = 532$ nm, TM (X-pol.) polarized light varying d (case b)

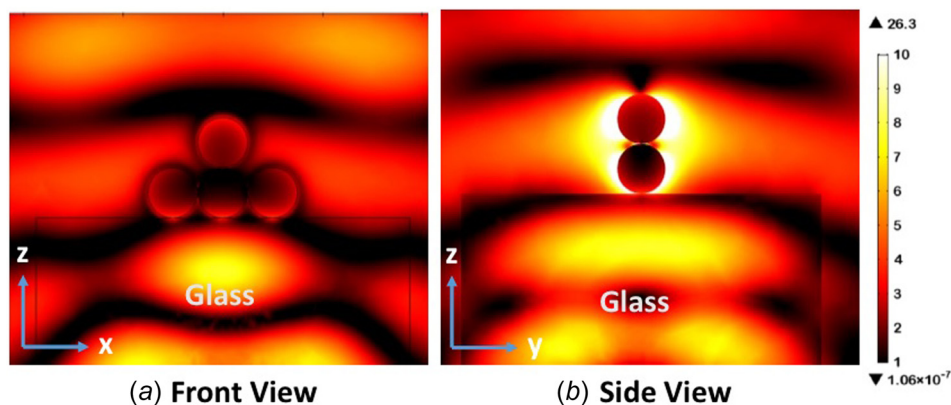


Fig. 5 Electric Field Enhancement $|E/E_0|$ with $\lambda = 532$ nm, TE polarized (Y-pol.) light with $d = 0$ (case b)

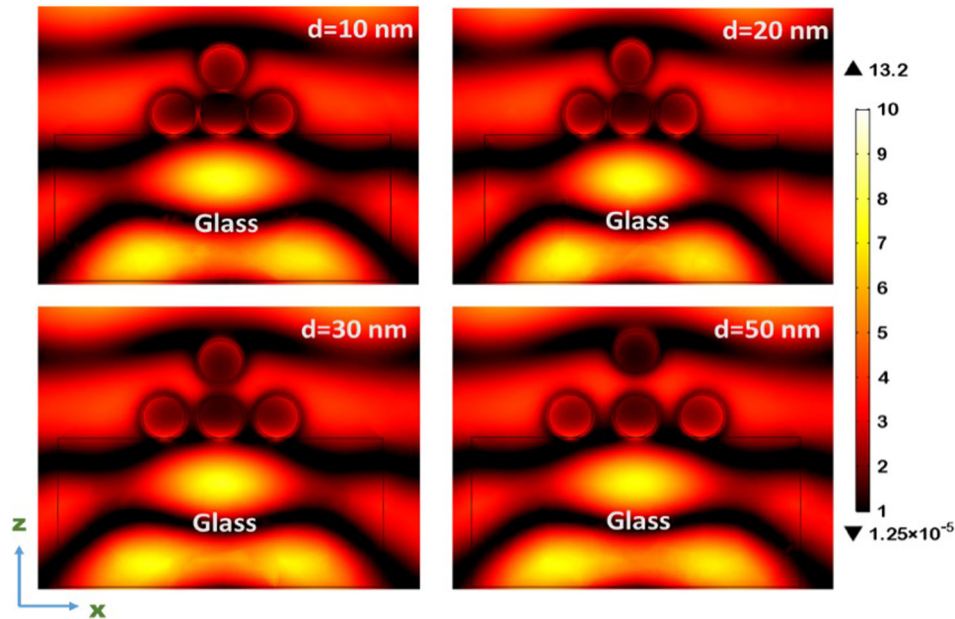


Fig. 6 Electric field enhancement $|E/E_0|$ with $\lambda = 532$ nm, TE polarized (Y-pol.) light with varying d (case b)

direction of the polarization on the particles. This is important because it implies that the particles in multilayer case are mostly affected by the layers close to the light source and that the effects of the plasmonic particles between the layers decrease through the bottom layers when illuminated by TE polarized light.

Figure 6 illustrates the electric field enhancement with varying d from 10 nm to 50 nm for the TE polarized light. It can be seen that the localized field enhancement is approximately constant at around 5–6 times when d is varied between 10 nm and 50 nm. Due to the polarization direction, the particle above the three bottom particles in a linear configuration does not significantly affect the bottom layer particles. This indicates that light/nanostructure interaction in this geometry is not affected significantly by the distance between the particles. Also, these results show that the enhanced field is always significantly greater for TM polarization than for the TE polarization for the 3D particle configurations where the particles are all in contact with each other but that the difference in the enhanced fields drops significantly when the particles start to have some spacing between each other. This indicates that the energy transfer between the particles is more significantly affected by the light for polarization when the particles are clustered together (i.e., $d=0$). Another interesting observation is that when the particle's distance, d , is on the order of the particle diameter, the field enhancement is almost the same for TE and TM configurations which implies that particles start to lose their near-field interactions at this scale and start to behave similarly for these cases.

Thermo-Optical Analysis of the Three-Dimensional Particle Structures. As the light is absorbed and scattered by the metallic nanoparticle at 532 nm wavelength, absorption and scattering cross sections were analyzed for TM (X-pol.) and TE (Y-pol.) polarized light.

It can be seen from Fig. 7 that absorption increases slightly with particle spacing for TE polarized light. The maximum electric field enhancement under TE polarized light depends only weakly on particle spacing. This slight increase in enhancement is due to the effect of the glass substrate on the nanoparticle placed above the three bottom particles in the linear configuration. Indeed, the background field on a glass substrate interferes with the absorption of the nanoparticle although this absorption increase is small. However, the absorption cross section decreases

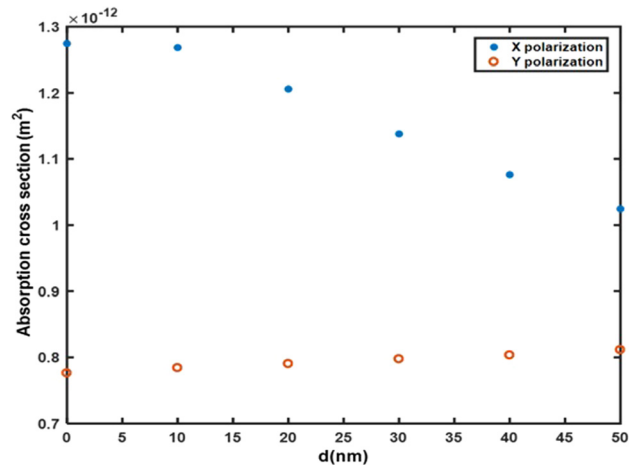


Fig. 7 Absorption cross section (m²) versus particle spacing (d)

when d is varying from 0 to 50 nm under TM polarized light. This can be explained as the collective properties of the linear nanoparticle array packing and the charge transport are along the polarization direction, which results in near-field confinement of the charge distribution with interference effect between the particles [36]. Hence, this effect starts to decrease as the gap increases which results in less absorption by the nanoparticles. We can also see that at large spacing, the particles act more as individual particles and the absorption cross section is expected to converge when d exceeds 50 nm with TM and TE polarized light.

Figure 8 shows the scattering cross section as a function of particle spacing. The scattering cross section decreases when d increases when illuminated with TE polarized light. This occurs because the particle configuration is orthogonal to the polarization direction resulting in relatively weak coupling to between the particles. In addition, the glass substrate tends to scatter more when the particles are packed closer together, as determined by analysis of the background field. However, this is not the case for TM polarized light because high near-field coupling with the evanescent waves between the nanoparticles in the regime of 0–10 nm

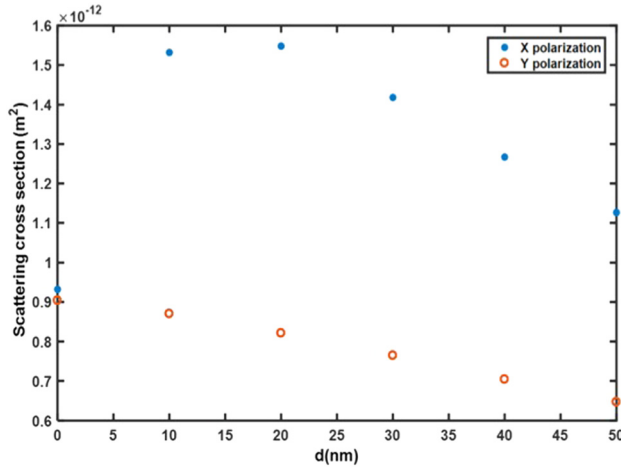


Fig. 8 Scattering cross section (m^2) versus particle spacing (d)

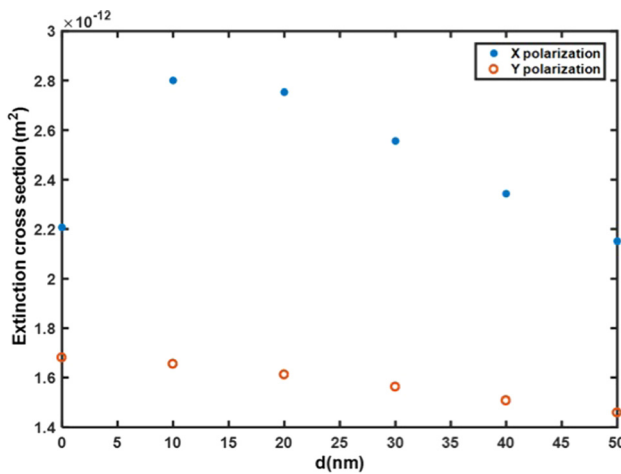


Fig. 9 Extinction cross section (m^2) versus particle spacing (d)

results in high scattering [31,37]. This near-field coupling starts to decrease linearly after d exceeds 20 nm. Furthermore, it is observed that the background field does not contribute on the nanoparticle scattering and a resonant scattering results in asymmetric line shape for TM polarized light.

Figure 9 shows the extinction cross section which is the sum of the absorption and scattering cross sections for both polarizations. It can be seen that the scattering cross section is dominant over the absorption cross section for the TM polarization. Hence, the trends in the extinction cross section as a function of d mirror that of the scattering cross section. As the decrease rate in the scattering cross section is more than increase rate of absorption cross section for TE polarization, the extinction cross section also decreases with d . It can also be seen from the single-scattering albedo analysis with particle spacing (d) in Fig. 10 that the absorption cross section contributes more to the extinction cross section for TE polarized light when d increases from 10 nm to 50 nm. This is also the case for TM polarization illumination, but this starts when d exceeds 30 nm. This is due to very intense near-field coupling between the nanoparticles, which results in strong scattering when the gap spacing is very small (<10 nm). Moreover, when the particles are at clustered together ($d=0$), the absorption cross section is dominant over the scattering due to the electromagnetic absorption by collective mode.

The extinction cross section analysis also shows that TM polarized light does not penetrate as far into the glass substrate

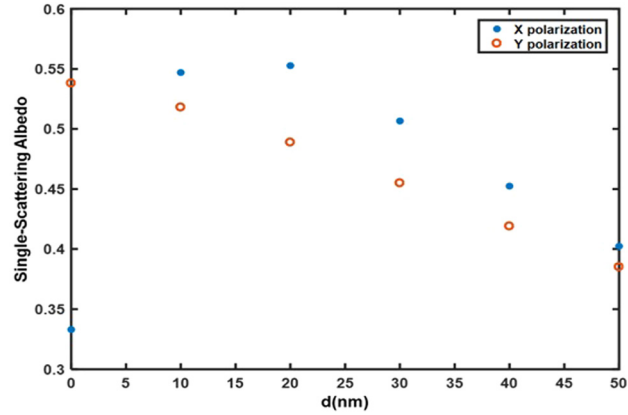


Fig. 10 Single-scattering Albedo versus particle spacing (d)

compared to the TE polarized light since the light is more quickly attenuated for TM polarized light. This indicates a greater degree of opacity (optically thicker) for TM polarized light than for TE polarized light with this nanoparticle configuration and optical wavelength. In addition, due to interference effects in the $d=0-10$ nm range, the attenuation results in an asymmetric behavior for TM polarized light. Overall, this result is important because the extinction cross section is related to how far the light energy can penetrate through the nanoparticles which will affect the depth of the sintering in the nanoparticle assemblies.

Figures 11 and 12 depict the time-averaged energy flux density per unit area (W/m^2), which shows the instantaneous power flow due to instantaneous electric and magnetic field distribution with varying d under 532 nm TM and TE polarized light, respectively.

For the TM polarization, when $d=0$ the Poynting vector is confined to mostly between the particles. In addition, when d increases from 20 nm to 50 nm, the particle above the linearly configured particles start to diminish the directed energy density flux with the particles located below. Also, we can see from Fig. 12 that the average of the instantaneous Poynting vector over time does not change significantly with varying d . This is expected because we do not observe highly confined coupling between the nanoparticles on a glass substrate for TE polarized light as discussed in the Multiparticle Analysis and Effect of Interparticle Spacing for TE Polarized Light section. However, it can be seen that the directed energy density is mostly between the nanoparticles and the glass substrate.

Figure 13 shows total resistive heating loss in the nanoparticles on the glass substrate. In the TM polarization case, the collective properties of the nanoparticles and the charge transport are along the polarization direction which results in high near-field confinement between the particles. This effect starts to decrease as the gap increases which results in less absorption by the nanoparticles for TM polarization. However, this is not the case for the TE polarized light because there is not high confinement between the particles, and the background field on glass substrate interferes the absorption of the nanoparticle. This results in higher absorption yet minimum increase with increasing d .

Overall, these results show that the configuration and spacing of the particles on the substrate can have a significant effect on the absorption and scattering of the light by the nanoparticles in the nanoparticle assembly. Therefore, the exact locations of the particles in the nanoparticle assembly will significantly change how the nanoparticle assembly heats up and the particles sinter together. In addition, the polarization of the light has a significant effect on both the extinction cross section as well as the resistive heating in the nanoparticle packings. Therefore, the selection of the correct laser source will have a major impact on the nanoparticle sintering process. These results also do give some insights into how we will expect the full nanoparticle assemblies to behave. For example, these results show that the maximum

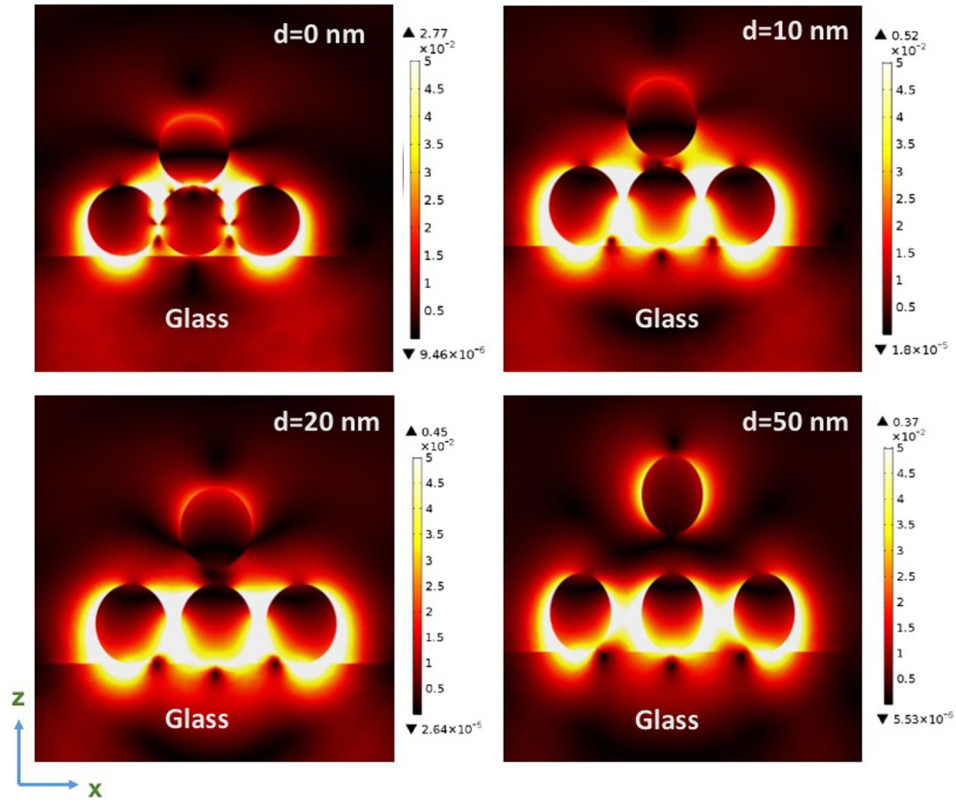


Fig. 11 Time-averaged Poynting vector (W/m^2) on the glass substrate and the air medium of the nanoparticles (case b) under $\lambda = 532$ nm, TM (X-pol.) polarized light

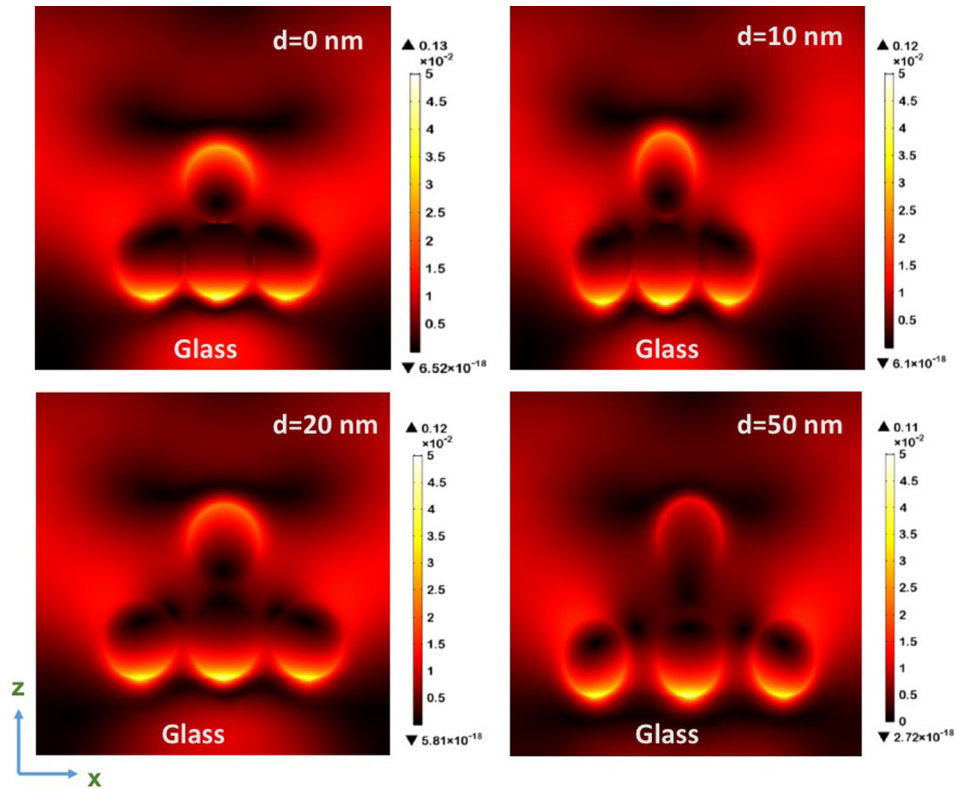


Fig. 12 Time-averaged Poynting vector (W/m^2) on the glass substrate and the air medium of the nanoparticles (case b) under $\lambda = 532$ nm, TE (Y-pol.) polarized light

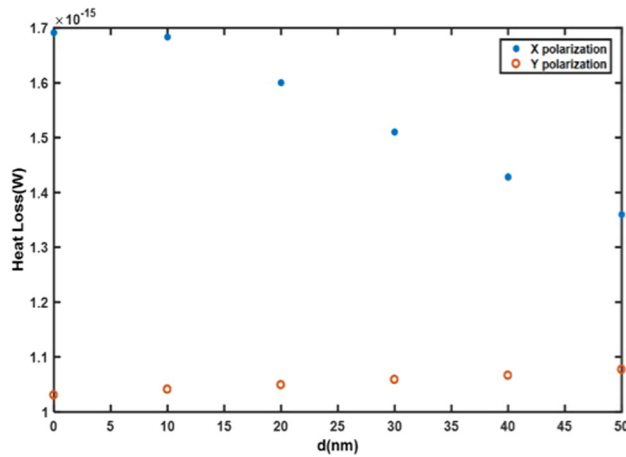


Fig. 13 Total resistive heating loss in the nanoparticles on a glass substrate under $\lambda = 532$ nm light with varying (d)

plasmonic enhancement and resistive heating occur when the particles in the assembly are in contact with each other. This is critical because sintering between particles can only occur where the particles are in contact with each other. The plasmonic enhancement at the interface between particles can, therefore, allow sintering to occur at temperatures well below the melting temperature. This result matches well with previous experimental results where the photonic sintering of copper nanoparticles is observed to occur at laser powers well below what would be required to fully melt the nanoparticles [38]. This means that local diffusion at the interface between the particles can be the dominant source of powder bed fusion in nanoparticle systems due to the very local plasmonic enhancement and heat generation where as microparticle-based additive manufacturing systems typically require the full melting of the particle to occur before particle fusion can take place [39]. Therefore, these local plasmonic enhancements between nanoparticles in microscale additive manufacturing processes, such as the microscale selective laser sintering process, allow parts to be manufactured at much lower bed temperatures then are required for more conventional selective laser sintering systems which helps to reduce the residual stress in the parts fabricated and allows additively manufactured structures to be fabricated on a wider variety of low temperature substrates.

The results for these 3D nanoparticle configurations indicated that a more detailed analysis of larger, random particle assemblies is required in order to be able to accurately predict the thermo-optical properties of full nanoparticle assemblies. These results will also need to be compared with the experimental results since the exact configuration of the particles in the assembly with respect to both the light polarization direction and the spacing between particles will dominate these assembly properties.

Conclusion

We have shown that solutions of Maxwell's equation in frequency domain can be used to analyze near-field interactions for nanoparticle sintering in 3D nanoparticle packings. We showed that the effect of the spacing between the nanoparticles with TE and TM polarizations is significant and observed that the field enhancement is highly dependent on the nanoparticle spacing. Also, it was determined that the maximum electric field enhancement is achieved when nanoparticles cluster together in a configuration where all the nanoparticles touching each other and that the enhancement decreases as the particle spacing increases. The thermo-optical properties change nonlinearly in the $d = 0-10$ nm regime due to the strong, nonlocal near-field interaction between the particles with the TM polarized light. This indicates that the different light polarizations result in different subwavelength energy transport mechanisms. These observations are, therefore,

an important step toward to understand photonic sintering between the particles for subwavelength 3D electronic structures.

References

- [1] Niittynen, J., Sowade, E., Kang, H., Baumann, R. R., and Mäntysalo, M., 2015, "Comparison of Laser and Intense Pulsed Light Sintering (IPL) for Inkjet-Printed Copper Nanoparticle Layers," *Sci. Rep.*, **5**, p. 8832.
- [2] Hwang, H. J., Oh, K. H., and Kim, H. S., 2016, "All-Photonic Drying and Sintering Process Via Flash White Light Combined With Deep-UV and Near-Infrared Irradiation for Highly Conductive Copper Nano-Ink," *Sci. Rep.*, **6**, p. 19696.
- [3] Cheng, C. W., and Chen, J. K., 2016, "Femtosecond Laser Sintering of Copper Nanoparticles," *Appl. Phys. A*, **122**(4), p. 289.
- [4] Paeng, D., Yeo, J., Lee, D., Moon, S. J., and Grigoropoulos, C. P., 2015, "Laser Wavelength Effect on Laser-Induced Photo-Thermal Sintering of Silver Nanoparticles," *Appl. Phys. A*, **120**(4), pp. 1229–1240.
- [5] Mubeen, S., Zhang, S., Kim, N., Lee, S., Krämer, S., Xu, H., and Moskovits, M., 2012, "Plasmonic Properties of Gold Nanoparticles Separated From a Gold Mirror by an Ultrathin Oxide," *Nano Lett.*, **12**(4), pp. 2088–2094.
- [6] Shen, S., Narayanaswamy, A., and Chen, G., 2009, "Surface Phonon Polaritons Mediated Energy Transfer Between Nanoscale Gaps," *Nano Lett.*, **9**(8), pp. 2909–2913.
- [7] Klar, T., Permer, M., Grosse, S., Von Plessen, G., Spirkl, W., and Feldmann, J., 1998, "Surface-Plasmon Resonances in Single Metallic Nanoparticles," *Phys. Rev. Lett.*, **80**(19), pp. 4249–4252.
- [8] Chen, G., 2005, *Nanoscale Energy Transport and Conversion: A Parallel Treatment of Electrons, Molecules, Phonons, and Photons*, Oxford University Press, Oxford, UK.
- [9] Bugada Miguel Cervera, G., and Lombera, G., 1999, "Numerical Prediction of Temperature and Density Distributions in Selective Laser Sintering Processes," *Rapid Prototyping J.*, **5**(1), pp. 21–26.
- [10] Dong, L., Makradi, A., Ahzi, S., and Remond, Y., 2009, "Three-Dimensional Transient Finite Element Analysis of the Selective Laser Sintering Process," *J. Mater. Process. Technol.*, **209**(2), pp. 700–706.
- [11] Kolossov, S., Boillat, E., Gardon, R., Fischer, P., and Locher, M., 2004, "3D FE Simulation for Temperature Evolution in the Selective Laser Sintering Process," *Int. J. Mach. Tools Manuf.*, **44**(2), pp. 117–123.
- [12] Nelson, J. C., Xue, S., Barlow, J. W., Beaman, J. J., Marcus, H. L., and Bourell, D. L., 1993, "Model of the Selective Laser Sintering of Bisphenol-A Polycarbonate," *Ind. Eng. Chem. Res.*, **32**(10), pp. 2305–2317.
- [13] Patil, R. B., and Yadava, V., 2007, "Finite Element Analysis of Temperature Distribution in Single Metallic Powder Layer During Metal Laser Sintering," *Int. J. Mach. Tools Manuf.*, **47**(7), pp. 1069–1080.
- [14] Singh, A. K., and Srinivasa Prakash, R., 2010, "Response Surface-Based Simulation Modeling for Selective Laser Sintering Process," *Rapid Prototyping J.*, **16**(6), pp. 441–449.
- [15] Tontowi, A. E., and Childs, T. H. C., 2001, "Density Prediction of Crystalline Polymer Sintered Parts at Various Powder Bed Temperatures," *Rapid Prototyping J.*, **7**(3), pp. 180–184.
- [16] Williams, J. D., and Deckard, C. R., 1998, "Advances in Modeling the Effects of Selected Parameters on the SLS Process," *Rapid Prototyping J.*, **4**(2), pp. 90–100.
- [17] Coquard, R., and Baillis, D., 2004, "Radiative Characteristics of Opaque Spherical Particles Beds: A New Method of Prediction," *J. Thermophys. Heat Transfer*, **18**(2), pp. 178–186.
- [18] Kamiuto, K., 2005, "Correlated Radiative Transfer Through a Packed Bed of Opaque Spheres," *Int. Commun. Heat Mass Transfer*, **32**(1), pp. 133–139.
- [19] Singh, B. P., and Kaviany, M., 1992, "Modelling Radiative Heat Transfer in Packed Beds," *Int. J. Heat Mass Transfer*, **35**(6), pp. 1397–1405.
- [20] Howell, J. R., and Klein, D. E., 1983, "Radiative Heat Transfer Through a Randomly Packed Bed of Spheres by the Monte Carlo Method," *ASME J. Heat Transfer*, **105**(2), pp. 325–332.
- [21] Zhou, J., Zhang, Y., and Chen, J. K., 2009, "Numerical Simulation of Laser Irradiation to a Randomly Packed Bimodal Powder Bed," *Int. J. Heat Mass Transfer*, **52**(13), pp. 3137–3146.
- [22] Feng, Y. T., Han, K., Li, C. F., and Owen, D. R. J., 2008, "Discrete Thermal Element Modelling of Heat Conduction in Particle Systems: Basic Formulations," *J. Comput. Phys.*, **227**(10), pp. 5072–5089.
- [23] Tsory, T., Ben-Jacob, N., Brosh, T., and Levy, A., 2013, "Thermal DEM-CFD Modeling and Simulation of Heat Transfer Through Packed Bed," *Powder Technol.*, **244**, pp. 52–60.
- [24] Widenfeld, G., Weiss, Y., and Kalman, H., 2003, "The Effect of Compression and Preconsolidation on the Effective Thermal Conductivity of Particulate Beds," *Powder Technol.*, **133**(1), pp. 15–22.
- [25] Zhang, H. W., Zhou, Q., Xing, H. L., and Muhlhaus, H., 2011, "A DEM Study on the Effective Thermal Conductivity of Granular Assemblies," *Powder Technol.*, **205**(1), pp. 172–183.
- [26] Bosbach, J., Martin, D., Stietz, F., Wenzel, T., and Träger, F., 1999, "Laser-Based Method for Fabricating Monodisperse Metallic Nanoparticles," *Appl. Phys. Lett.*, **74**(18), pp. 2605–2607.
- [27] Kuznetsov, A. I., Kiyon, R., and Chichkov, B. N., 2010, "Laser Fabrication of 2D and 3D Metal Nanoparticle Structures and Arrays," *Opt. Express*, **18**(20), pp. 21198–21203.
- [28] Yuksel, A., and Cullinan, M., 2016, "Modeling of Nanoparticle Agglomeration and Powder Bed Formation in Microscale Selective Laser Sintering Systems," *Addit. Manuf.*, **12**(Part B), pp. 204–215.
- [29] Li, L., Hong, M., Schmidt, M., Zhong, M., Malshe, A., Huis, B., and Kovalevko, V., 2011, "Laser Nano-Manufacturing—State of the Art and Challenges," *CIRP Annals-Manuf. Technol.*, **60**(2), pp. 735–755.

- [30] Sosa, I. O., Noguez, C., and Barrera, R. G., 2003, "Optical Properties of Metal Nanoparticles With Arbitrary Shapes," *J. Phys. Chem. B*, **107**(26), pp. 6269–6275.
- [31] Evlyukhin, A. B., Brucoli, G., Martín-Moreno, L., Bozhevolnyi, S. I., and García-Vidal, F. J., 2007, "Surface Plasmon Polariton Scattering by Finite-Size Nanoparticles," *Phys. Rev. B*, **76**(7), p. 075426.
- [32] Johnson, P. B., and Christy, R. W., 1972, "Optical Constants of the Noble Metals," *Phys. Rev. B*, **6**(12), pp. 4370–4379.
- [33] Hutter, T., Elliott, S. R., and Mahajan, S., 2012, "Interaction of Metallic Nanoparticles With Dielectric Substrates: Effect of Optical Constants," *Nanotechnology*, **24**(3), p. 035201.
- [34] Maier, S. A., Kik, P. G., and Atwater, H. A., 2003, "Optical Pulse Propagation in Metal Nanoparticle Chain Waveguides," *Phys. Rev. B*, **67**(20), p. 205402.
- [35] Sweatlock, L. A., Maier, S. A., Atwater, H. A., Penninkhof, J. J., and Polman, A., 2005, "Highly Confined Electromagnetic Fields in Arrays of Strongly Coupled Ag Nanoparticles," *Phys. Rev. B*, **71**(23), p. 235408.
- [36] Wang, Y., Duan, C., Peng, L., and Liao, J., 2014, "Dimensionality-Dependent Charge Transport in Close-Packed Nanoparticle Arrays: From 2D to 3D," *Sci. Rep.*, **4**, p. 7565.
- [37] Nicolas, R., Lévêque, G., Marae-Djouda, J., Montay, G., Madi, Y., Plain, J., and Maurer, T., 2015, "Plasmonic Mode Interferences and Fano Resonances in Metal-Insulator-Metal Nanostructured Interface," *Sci. Rep.*, **5**(1), p. 14419.
- [38] Zenou, M., Ermak, O., Saar, A., and Kotler, Z., 2013, "Laser Sintering of Copper Nanoparticles," *J. Phys. D Appl. Phys.*, **47**(2), p. 025501.
- [39] Roy, N. K., Yuksel, A., and Cullinan, M. A., 2015, " μ -SLS of Metals: Physical and Thermal Characterization of Cu-Nanopowders," Solid Freeform Fabrication Conference (SFF), Austin, TX, Aug. 7–9, pp. 772–788.